

Photoexcited breathers in conjugated polyenes: An excited-state molecular dynamics study

S. Tretiak[†], A. Saxena, R. L. Martin, and A. R. Bishop

Theoretical Division and Center for Nonlinear Studies, Los Alamos National Laboratory, Los Alamos, NM 87545

Communicated by Alan J. Heeger, University of California, Santa Barbara, CA, January 8, 2003 (received for review September 20, 2002)

π -conjugated polymers have become an important class of materials for electronic devices. Design of these devices requires understanding such processes as photochemical reactions, spatial dynamics of photoexcitations, and energy and charge transport, which in turn involve complex coupled electron-vibrational dynamics. Here we study nonlinear photoexcitation dynamics in the polyene oligomers by using a quantum-chemical method suitable for the simulation of excited-state molecular dynamics in extended molecular systems with sizes up to hundreds of atoms. The method is based on the adiabatic propagation of the ground-state and transition single-electron density matrices along the trajectory. The simulations reveal formation of a self-localized vibronic excitation (“breather” or multiquanta bound state) with a typical period of 34 fs and allows us to identify specific slow and fast nuclear motions strongly coupled to the electronic degrees of freedom. The effect of chain imperfections and chemical defects on the dynamics is also investigated. A complementary two-dimensional analysis of corresponding transition density matrices provides an efficient way to monitor time-dependent real-space localization of the photoexcitation by identifying the underlying changes in charge densities and bond orders. Possible correlated electronic and vibrational spectroscopic signatures of photoexcited breathers are predicted, and generalizations to energy localization in complex macromolecules are discussed.

The science and technology of electronic and optoelectronic devices based on organic π -conjugated polymers is evolving rapidly. Numerous high-performance photonic devices fabricated from organic polymers and molecular crystals have been made (1, 2), including light-emitting diodes (LEDs) (2–8) and electrochemical cells (9), display panels (10–12), photovoltaic cells (13–15), photodetectors (16–18), transistors (19–21), light-emitting field-effect transistors (22), biosensors (23), imaging devices (24, 25), and solid-state lasers (26–29). The rational design of novel plastic materials with enhanced functionalities requires insight into their electronic structure, charge and energy transport, and photoexcitation dynamics. This study has become a research frontier that involves many challenges for theory, experiment, and synthesis; however, a sufficient fundamental understanding is yet to be achieved.

The theoretical description of π -conjugated molecular systems is challenging because of electronic correlation effects and strong electron-phonon interactions. It is well understood from the early days of polyacetylene studies (1, 30) that coupling of the electrons to the nuclear degrees of freedom results in a very rich photophysics of solitons, polarons, and excitons and makes an important distinction of “soft” condensed matter from rigid solids based on semiconductor or crystalline metal materials. On the other hand, electron correlation effects have a dramatic impact on the electronic structure, leading, e.g., to the inverse ordering of $2A_g$ and $1B_u$ excited states in finite polyenes (31). The early studies conducted for finite systems in real space (32, 33) or for periodic lattices using one-dimensional band theories (k space) (34) were based on simple empirical Hamiltonian models such as Su-Schrieffer-Heeger (SSH) (30, 35) and made an invaluable contribution to our qualitative understanding of such phenomena.

However, an accurate description of molecular chemical structures including defects, disorder, and chemical substitutions is

beyond an empirical treatment but possible with quantum-chemical methods. The development of powerful computers and versatile program packages such as the Gaussian suite (36) leads to the growing importance of quantum chemistry for the understanding underlying fundamental electronic phenomena and for providing accurate predictions of relevant observables. For ground-state adiabatic potential surfaces (e.g., geometry optimization, transition-state searches, and molecular and reaction dynamics) these approaches are currently well developed. In most cases, ground-state wavefunctions can be well represented by a single Slater determinant (37), and this approximation allows the treatment of fairly large molecular systems. However, the computation of excited states requires accounting for electronic correlation effects by using, for example, a multiconfigurational representation (38), which is a numerically expensive procedure. Nevertheless, accurate computations of excited-state structures, UV-visible spectra, and nonlinear polarizabilities at the fixed optimal ground-state geometry are currently routine even for large molecules with sizes up to several hundred atoms (38, 39). Configuration interaction combined with semiempirical Hamiltonian models such as the intermediate neglect of differential overlap/spectroscopy (40) or the time-dependent density functional theory (41) are the most popular approaches for excited-states calculations, the former method being less expensive than the latter.

Computation of the excited-state *dynamical processes* that involve nuclear degrees of freedom still remains a computational challenge and is available only for small molecules. The recently developed excited-state molecular dynamics (ESMD) approach (42–44), schematically illustrated in Fig. 1, represents a reasonable compromise between accuracy and numerical effort and allows adiabatic photoexcitation dynamics to be followed on picosecond time scales in molecules with hundreds of atoms. This approach is based on the collective electronic-oscillator method (39), which combines the random-phase approximation for a many-electron problem (which includes essential electronic correlations) with a semiempirical Hamiltonian model [such as intermediate neglect of differential overlap/spectroscopy (45) or Austin model 1 (46)]. The collective electronic oscillator allows accurate prediction of spectroscopic observables by using fast Krylov-space diagonalization techniques to calculate excited states with minimal numerical effort (39). The ESMD utilizes the collective electronic oscillator approach to calculate gradients of the excited-state potential energy surface (forces) on the fly. These quantum-mechanical forces are used further to propagate classical Newtonian equations of motion for the nuclei to model the time-dependent vibronic evolution (42). This approach therefore is applicable within the Born-Oppenheimer approximation and allows treatment of adiabatic photoexcited dynamics.

In this article we investigate the excited-state electron-nuclear dynamics of a polyacetylene chain (which is a simple π -conjugated polymer and serves as a prototype of a one-dimensional electronic system with strong coupling to nuclear degrees of freedom). Our focus is on the formation of photoexcited “breathers,” i.e., multiquanta vibronic states. A breather is a dynamic state representing

Abbreviations: SSH, Su-Schrieffer-Heeger; ESMD, excited-state molecular dynamics.

[†]To whom correspondence should be addressed. E-mail: serg@lanl.gov.

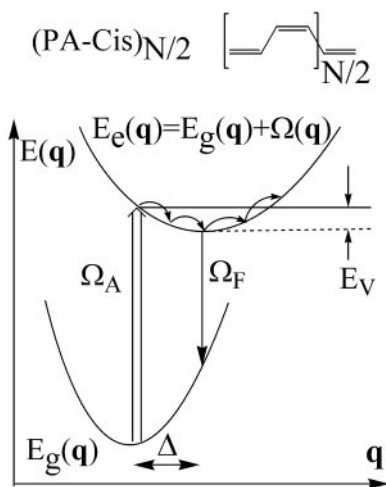


Fig. 1. Geometry of *cis*-polyacetylene and schematic representation of molecular dynamics propagation. The excited-state potential energy $E_e(\mathbf{q})$ as a function of nuclear coordinates \mathbf{q} , displacements Δ , vertical absorption Ω_A , and fluorescence Ω_F frequencies.

a spatially localized, time-persistent nonlinear excitation. Extensive studies based on SSH-type models predicted the formation of breather-like states in polyenes after either photoexcitation (32, 33, 47–49) or electronic ground-state perturbations of sufficient energy (50). A clear physical picture emerges, for example, for photoexcitation dynamics in *trans*-polyacetylene (which has two degenerate ground-state conformations): An electron-hole pair (exciton) created by an absorbed photon decays to a charged soliton–antisoliton pair. These quasiparticles rapidly become spatially separated on the time scale of a few tens of femtoseconds, whereas a part of the initial photoexcitation energy, which is left behind, forms a localized breather (33, 47). In polymers with a nondegenerate ground state such as *cis*-polyacetylene, this picture is more complicated: The exciton cannot decay into a fully separated soliton–antisoliton pair because of confinement effects. Instead, the composite dynamics of an electron, a hole and a breather, develops (48). In these models, the size of spatial localization strongly depends on the empirical Hamiltonian parameters (30, 35). These model investigations also attributed peaks near the $\pi - \pi^*$ edge region in the photoinduced absorption as a spectroscopic signature of breathers (47, 48, 51). However, it took almost two decades to develop ultrafast sub-5-fs experimental spectroscopic techniques to monitor real-time vibronic dynamics of conjugated polymers that may support the existence of breathers (52).

Although it is straightforward to treat practically any organic molecular structure (within certain size limits) with the ESMD method (39, 42, 43), we focus here on polyacetylene. This choice is for two reasons: (i) the ability to compare these calculations with early studies of breathers calculated within the empirical Hamiltonian models (32, 33, 47–49) and (ii) recent experimental evidence for breather excitations in polyacetylene (52). Our results reproduce all the essential features of the early studies and predict characteristic properties that do not depend on empirical Hamiltonian parameters. In addition, our results provide all the information necessary for modeling a variety of spectroscopic data, which allows us to connect these simulations with recent experiments (52) and to predict additional spectroscopic signatures of breathers. Finally, we study the dynamics in the presence of a structural defect (an acetylene bond) and chemical substitutions (halogenization) to understand the effect of chain imperfections on the photoexcitation dynamics.

Results and Discussion

We used the Austin model 1 Hamiltonian for all calculations presented in this article. Austin model 1 has been parameterized specifically to reproduce ground-state properties (such as chemical energy, geometry, dipole moment, etc.) in a variety of molecules (46). In addition, this model provides a reasonable accuracy for excited-state properties in combination with the random-phase approximation (53, 54). The calculations start from the optimal geometry of a linear *cis*-polyacetylene oligomer obtained with the standard GAUSSIAN 98 computational package (36), i.e., the ground-state potential energy $E_g(\mathbf{q})$ is minimal in the space of nuclear coordinates \mathbf{q} , which span the $3N - 6$ -dimensional space, with N being the total number of atoms in the molecule. We further use the ESMD computational package to follow photoexcitation adiabatic dynamics up to a 0.5-ps time scale (42). This approach calculates the excited-state potential energy as $E_e(\mathbf{q}) = E_g(\mathbf{q}) + \Omega(\mathbf{q})$. Here $\Omega(\mathbf{q})$ is the excitation frequency to the lowest $1B_u$ (band-gap) state of polyacetylene. The program uses numerical derivatives of $E_e(\mathbf{q})$ with respect to each nuclear coordinate q_i ($i = 1, \dots, 3N - 6$) to calculate forces and subsequently to step along the excited-state hypersurface using these gradients. A standard Verlet molecular dynamics algorithm (55) has been used for propagation of the Newtonian equations of motion. No dissipative processes are included here, so the total energy (initial ground-state energy plus the energy of the absorbed photon) is conserved in the simulations. In a separate simulation we introduced an artificial dissipative force into the equations of motion to obtain the minimum of the excited-state potential energy $E_e(\mathbf{q})$ corresponding to the relaxed geometry.

To analyze excited-state dynamics of *cis*-polyacetylene we calculate oligomers (with free boundary conditions) long enough ($n = 120$ carbon atoms) to mimic the infinite chain limit [typically spectroscopic observables in polyenes saturate to the bulk limit at 60–80 carbon atom chain lengths (38, 39)]. To monitor the vibrational dynamics we focus on the bond-length alternation parameter, which reflects an uneven distribution of the π electrons over the bonds (Peierls distortion) and is therefore strongly coupled to the electronic system. The bond-length alternation parameter r_n is defined as

$$r_n = (-1)^n(l_{n-1} - l_n), \quad n = 2, \dots, N - 1, \quad [1]$$

where l_n is the bond length between the n th and $n + 1$ th atoms along the chain. In addition, we define a local compression parameter s_n as

$$s_n = 2\Delta x_n + \Delta x_{n-1} + \Delta x_{n+1}, \quad n = 2, \dots, N - 1, \quad [2]$$

where Δx_n is the deviation of n th atom from its equilibrium position. The s_n parameter reflects the changes of the lattice constant. r_n and s_n have been defined in a similar fashion for the SSH Hamiltonian (47, 48).

To follow the electronic dynamics we further use a real-space two-dimensional representation of the transition density matrices (39). These matrix elements reflect the changes in electronic density and coherences and therefore characterize the properties of an exciton or bound electron-hole pair created after photoexcitation (39, 56). Transition densities are defined as

$$(\xi_\nu)_{ij} = \langle \nu | c_i^+ c_j | g \rangle, \quad [3]$$

where (c_j) are creation (annihilation) operators of an electron at the j th atomic orbital, and $|g\rangle$ ($|\nu\rangle$) is the ground (excited)-state many-electron wavefunction (39, 56). The diagonal elements $(\xi_\nu)_{jj}$ represent the net charge induced in the j th atomic orbital by the external field. The off-diagonal elements $(\xi_\nu)_{ij}$ with $i \neq j$ represent the joint probability amplitude of finding an electron

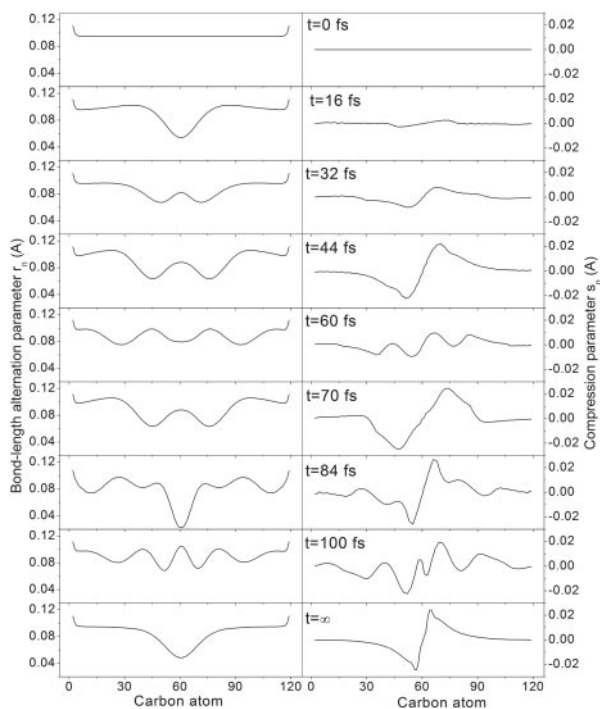


Fig. 2. Variation of bond-length alternation [r_n (Å)] and compression [s_n (Å)] parameters in (polyacetylene-*cis*)₆₀ oligomer along the polymer's backbone at $t = 0, 16, 32, 44, 60, 70, 84, 100,$ and ∞ fs after photoexcitation. $t = 0$ corresponds to absorption (fluorescence) events for the molecule being at the ground (excited)-state equilibrium geometry.

and a hole located at the i th and j th atomic orbitals, respectively. Thus, a transition density plot depicts probabilities of an electron moving from one molecular position (horizontal axis) to another (vertical axis) after electronic excitation.

Fig. 2 shows the variation of r_n and s_n , and Fig. 3 displays the correspondent transition densities at specific times up to 100 fs. At the moment of photoexcitation ($t = 0$) the molecule in the ground state has a constant dimerization ($r_n = 0.095$ Å) and s_n is vanishing along the polymer chain (i.e., there is no variation in lattice constant). The effects from the molecular ends are small and local. Therefore, after the photoexcitation, the exciton created is initially delocalized along the entire chain (Fig. 3, $t = 0$). The diagonal direction of the plot shows the coordinate of the exciton's center of mass measured by the delocalization size L_d , which is distributed evenly among all carbon atoms (except the molecular ends) at $t = 0$. The size of the exciton (maximum distance between an electron and a hole), which is characterized by the off-diagonal extent of the plot (measured by the coherence size L_c), is ≈ 20 – 25 carbon atoms and is much smaller than the oligomer length.

Because of strong coupling to vibrational degrees of freedom (electron–phonon coupling) an exciton rapidly distorts the lattice in the middle of the chain (Fig. 3, $t = 16$ fs), locally reducing the bond-length alternation (Fig. 2, $t = 16$ fs), and localizes itself in this region on the time scale of ≈ 20 fs. This exciton self-trapping process is typical for one-dimensional conjugated polymers (30, 42, 43). When an exciton distorts the lattice, dynamical vibrational excitations (phonons) are created, appearing as waves in r_n and s_n on the edges of the exciton potential well (Fig. 2, $t = 16$ fs). The subsequent dynamics can be qualitatively described as: the phonon “waves” propagate in opposite directions, reflect from the chain ends, and finally meet in the middle of the chain (Fig. 2, $t = 32$ fs), pulling an exciton out of its well and delocalizing the excitation (Fig. 3, $t = 32$ fs). The exciton, in turn, attempts to localize again, creating more phonons, i.e., the energy is exchanging between electronic and

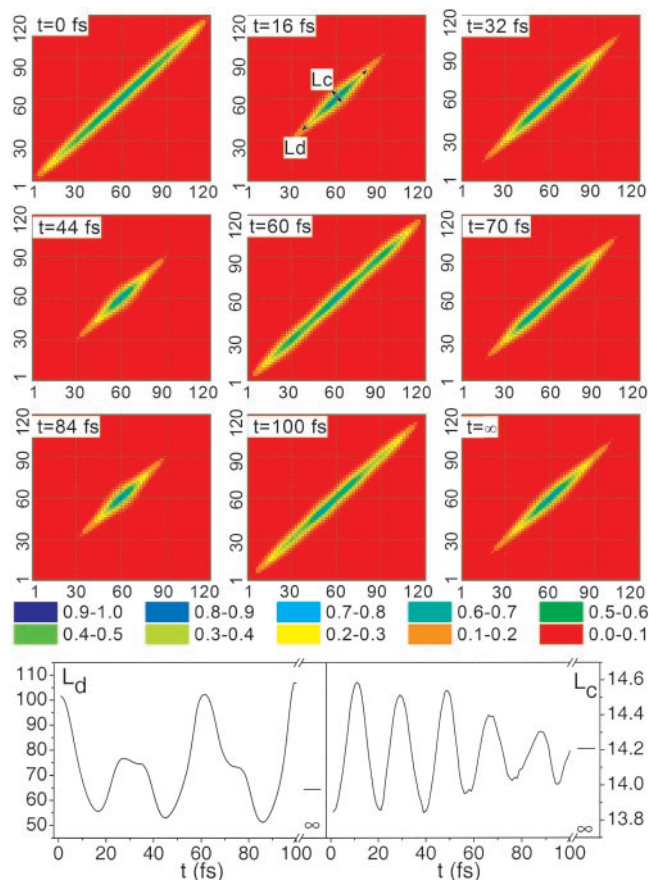


Fig. 3. (Upper) Contour plots of the transition densities between the ground state ($|0\rangle$) and the first excited $1B_u$ state ($|1\rangle$) in (polyacetylene-*cis*)₆₀ oligomer at $t = 0, 16, 32, 44, 60, 70, 84, 100,$ and ∞ fs after photoexcitation. The axes are labeled by the carbon atoms along the chain. The color map is given on the bottom of the color plots. (Lower) Variation of the diagonal (L_d) and off-diagonal (L_c) coherence sizes in carbon atoms with time. Equilibrium values of these quantities at excited-state relaxed geometry ($t = \infty$) are also shown. L_c and L_d define, respectively, the sizes of the exciton and localization of the exciton on the polymer backbone.

vibrational degrees of freedom. Subsequently, the magnitudes of r_n and s_n increase, and the nuclear dynamics becomes more complex because more vibrational modes are involved (Fig. 2, $t = 44, 60, 70, 84,$ and 100 fs). In agreement with refs. 47 and 48, we also notice that s_n roughly behaves as a derivative of r_n , even though these are formally unrelated parameters corresponding to slow (acoustic) and fast (optical) phonons, respectively. The electronic dynamics in turn mirrors structural deformations by exciton delocalization in the regions with the lower bond-length alternation (Fig. 3, $t = 44, 60, 70, 84,$ and 100 fs). This variation of diagonal delocalization is a characteristic “breathing” pattern. The overall electron–nuclear dynamics is a nonlinear and nonperiodic (on relevant femtosecond–picosecond time scales) process, because all vibrational degrees of freedom are coupled to electronic structure and to each other. The most significant structural changes occur in the middle of the chain, which can be envisioned as a localized and persistent vibrational excitation or a breather, i.e., we observe coupled nonlinear dynamics of collective electronic (electron and hole) and lattice (breather) excitations. A similar process has been observed in simulations with a simple SSH model (48). However, there is an important distinction from these early studies: The nuclear dynamics of a real polymer is far richer and more complex than the dynamics of one-dimensional lattice. Finally, if dissipation is introduced, the exciton is localized in the middle of the chain in a region with reduced bond-length alternation over ≈ 30 -carbon-atoms length,

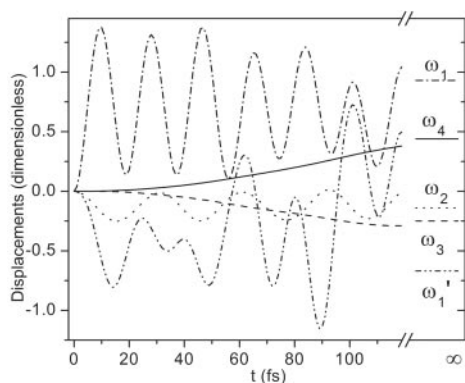


Fig. 4. Variation of dimensionless displacements along selected vibrational normal modes with time. These nuclear motions strongly couple to the electronic degrees of freedom and can be interpreted as C=C ($\omega_1 = 1,825.8 \text{ cm}^{-1}$ and $\omega_1' = 1,826.8 \text{ cm}^{-1}$) and C—C ($\omega_2 = 1,079.8 \text{ cm}^{-1}$) stretches (fast modes), polymer backbone stretch ($\omega_3 = 101.2 \text{ cm}^{-1}$), and wagging motion ($\omega_4 = 61.2 \text{ cm}^{-1}$) (slow modes). Equilibrium values of these quantities at the excited-state relaxed geometry ($t = \infty$) are also shown.

which formally corresponds to the long-time limit (Figs. 2 and 3, $t = \infty$ fs).

To quantitatively characterize the time scales of the exciton dynamics, we calculated the diagonal (L_d) and off-diagonal (L_c) exciton coherence sizes as respective inverse participation ratios (following ref. 39). Variation of L_d and L_c with time is shown in Fig. 3 *Bottom*. These quantities vary quasiperiodically with typical periods of ≈ 34 fs (L_d) and ≈ 18 fs (L_c) determined from their power spectra (not shown). We also notice that the magnitude of L_d changes considerably (by $\approx 50\%$), whereas L_c does not vary significantly, i.e., photoexcitation dynamics affects the spatial localization of an electron-hole pair but not the exciton size.

To relate these time scales to molecular vibrations, we calculated vibrational normal modes for the ground-state equilibrium geometry and expanded the excited-state structural changes in the basis set of these coordinates to obtain dimensionless displacements Δ_i ($i = 1, \dots, 3N - 6$). We find that many fast and slow nuclear modes have significant displacements and therefore are dynamically coupled to the electronic system. The variation in the displacements for the most pronounced molecular vibrations are shown in Fig. 4. Vibrational modes with frequencies $\omega_1 = 1,825.8$ and $\omega_1' = 1,826.8 \text{ cm}^{-1}$ are related to “in-phase” and “out-of-phase” C=C stretches and overall have positive and negative displacements, respectively, corresponding to an elongated double bond. These modes most resemble phonons with $k = 0$ and 2 momenta in the long-chain limit, respectively, with typical periods of 18.3 fs. Displacements corresponding to these nuclear motions show quasiperiodic variations around their relaxed values. There are several other quasiperiodic C=C stretching modes related to the optical phonon band in the long-chain limit. We observe that C=C stretching modes corresponding to phonons with higher momenta have consequently smaller displacements (note that phonons with odd momenta do not contribute to the dynamics because the inversion symmetry is preserved during the simulations). Another fast nuclear motion corresponding to the C—C stretch ($\omega_2 = 1,079.8 \text{ cm}^{-1}$) has an overall negative displacement (shorter single bond) and a period of 30.9 fs. In addition, several vibrational modes corresponding to the slow motion with typical periods of a few hundreds femtoseconds are also strongly coupled to the electronic system. Variation of the displacements of two slow modes with frequencies 61 and 101 cm^{-1} are shown in Fig. 4. The same types of vibrational modes with similar couplings to the electronic system have been identified in a study of excited-state potentials of short polyenes ($n = 8\text{--}20$ carbon

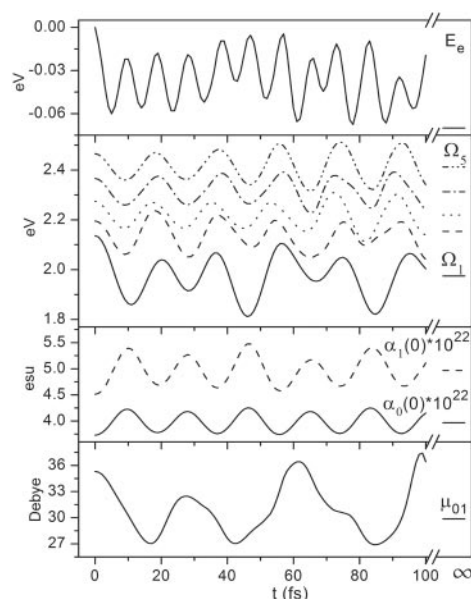


Fig. 5. Variation of electronic potential energy E_e , transition frequencies of the first five electronic excited states, $\Omega_1 - \Omega_5$, ground $\alpha_0(0)$ and excited $\alpha_1(0)$ state static polarizabilities, and transition dipole μ_{01} between the ground state ($|0\rangle$) and the first excited $1B_u$ state ($|1\rangle$) with time. Equilibrium values of these quantities at the excited-state relaxed geometry ($t = \infty$) are also shown.

atoms) by using a configuration interaction/semiempirical approach (57).

As expected, the L_c variation is related to C=C stretches, which reflects the dependence of the exciton size on the bond-length alternation measuring the degree of Peierls dimerization. However, we notice that the L_d period of ≈ 34 fs does not correspond to any normal mode with a significant displacement, i.e., the L_d variation is related to a collective localized vibrational excitation (breather) that cannot be represented by a linear vibrational phonon mode.

We next analyze the time dependence of several observables (Fig. 5) to study possible spectroscopic signatures of the vibronic dynamics described above. Fig. 6 shows power spectra that identify the relevant frequency components. We expect that the signatures of C=C stretching motions, which show the strongest coupling to the electronic system (Fig. 4), will be the most pronounced. The excited-state potential energy E_e varies with a period of ≈ 9 fs, which is related to a doubled frequency of the C=C stretching motion. This could be interpreted even within a simple model that assumes that the excited-state energy has an elastic harmonic term $Ku^2/2$,

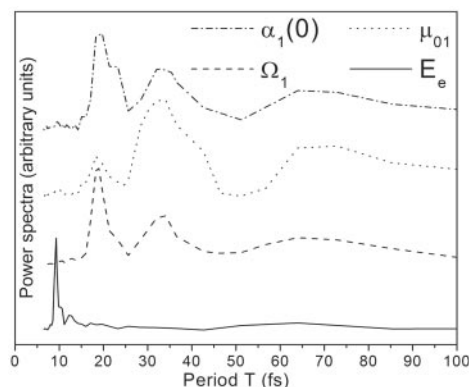


Fig. 6. Power spectra of electronic potential energy E_e , transition frequency Ω_1 , excited-state static polarizability $\alpha_1(0)$, and transition dipole μ_{01} .

with K being the spring constant and $u \approx \sin(\omega_1 t)$ the atomic displacement. It then is clear that E_c will vary with a frequency of $2\omega_1$.

Variations of transition frequencies are also coupled to C=C stretching motions that change the bond-length alternation with an ≈ 18 -fs period (Fig. 5). It is instructive to draw a connection with solid-state band theories, which show that the band-gap energy (which corresponds to the Ω_1 transition frequency) has a component βu from the Peierls distortion, with β being the electron-phonon coupling constant and $u \approx \sin(\omega_1 t)$. We notice that the magnitude of frequency variations decreases for the higher energy electronic states, which are more localized as compared with the band-gap state and therefore less sensitive to the bond-length alternation variations. In addition, the power spectrum of Ω_1 has weaker frequency components at ≈ 34 and ≈ 70 fs (Fig. 6), which cannot be associated with any specific vibrational mode. Similarly, the ground [$\alpha(0)$] and excited [$\alpha(1)$] state polarizabilities (calculated as the second derivatives of the ground- and excited-state energies, respectively) have an ≈ 18 -fs period varying with phase opposite to that of the transition frequencies. This can be rationalized by recalling that in a single-state approximation, the polarizability is inversely proportional to the square of the transition energy $\alpha = f/\Omega^2$, with f being the oscillator strength. The power spectra of polarizabilities also contain ≈ 34 - and ≈ 70 -fs components (Fig. 6).

We next calculate the transition dipole moment between ground and excited states as the expectation value of the dipole operator μ : $\mu_{01} = \text{Tr}(\mu \xi_1)$. This quantity, and subsequently the correspondent oscillator strength (not shown), are dominated by an ≈ 34 -fs period (see Fig. 5), which corresponds to the breather excitation, and weaker ≈ 18 - and ≈ 70 -fs components. For the delocalized band-gap excitations each segment of the polymer chain along the L_d length contributes almost equally to the oscillator strength, which leads to overall scalings $\mu_{01} \approx \sqrt{n}$ and $f_{01} \approx n$. Thus, changes in the diagonal delocalization size L_d cause variation of the transition dipole and the oscillator strength. Vibronic spectroscopy of small molecules is typically described by using the Condon approximation, which implies that the transition dipole does not change in the course of photoexcitation dynamics. However, the significant changes in the transition dipole magnitude we observe in the present case show that the Condon approximation is not always applicable for extended molecular systems. Variation of the transition dipole is an important signature of the breather vibrational excitations, which may be detected spectroscopically.

In summary, the power spectra of all spectroscopic observables (transition frequency, transition dipole, and polarizability) contain clear frequency components with periods of ≈ 18 , ≈ 34 , and ≈ 70 fs. Only the ≈ 18 -fs harmonic is related to C=C stretching vibrational normal mode ($\omega_1 \approx 1,826 \text{ cm}^{-1}$), whereas the other two harmonics are not associated with the vibrational spectrum, with ≈ 34 fs being the breather excitation.

To explore the effect of defects and chain imperfections on photoexcitation dynamics we simulated a *cis*-polyacetylene oligomer that contains an alkynyl (triple-bond) chemical defect. The resulting variations of r_n , s_n , and transition densities are shown in Fig. 7 Upper. We first notice that the triple bond is a very weak defect that does not break the conjugation but locally increases the bond-length alternation. Therefore, initially (Fig. 7, $t = 0$) an exciton is still delocalized along the entire molecule, which is similar to pristine polyacetylene (compare with Fig. 3, $t = 0$). However, the dynamics is very different: Immediately an exciton moves to the most conjugated part of the chain, and all subsequent vibronic dynamics, which includes breather formation, occurs on this segment with weak penetration of an excitation to the neighboring segment (Fig. 7). This is the natural relaxation of our photoexcitation to the lowest $\pi - \pi^*$ electronic state, which lies in the largest conjugation segment of the chain. The defect provides a strong impedance mismatch, localizing the excited energy. Of course,

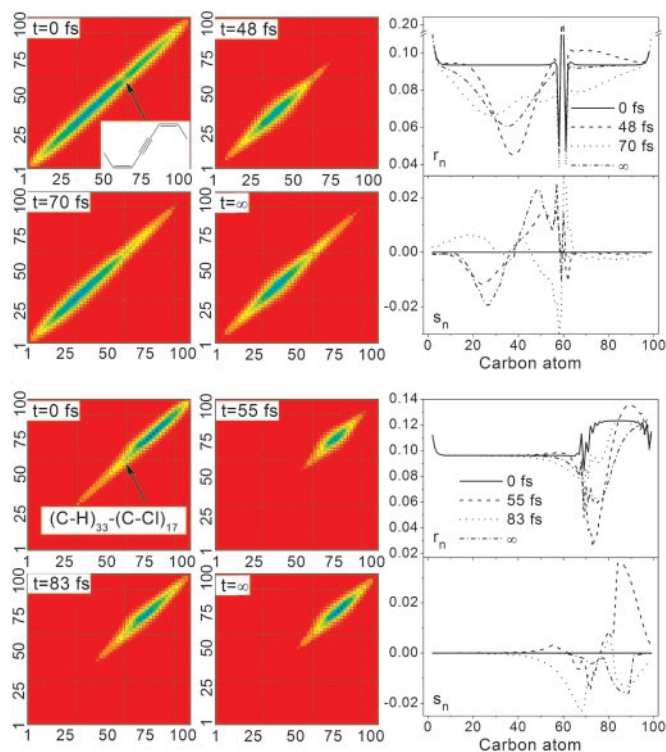


Fig. 7. (Upper) The effect of alkynyl (triple-bond) defect in (polyacetylene-*cis*)₅₀ oligomer on photoexcitation dynamics. (Left) Contour plots of the transition densities between the ground state ($|0\rangle$) and the first excited $1B_u$ state ($|1\rangle$) at $t = 0, 44, 70$, and ∞ fs. (Right) Variation of bond-length alternation [r_n (Å)] and compression [s_n (Å)] parameters along the polymer backbone at $t = 0, 44, 70$, and ∞ fs. (Lower) The effect of halogenization (chlorine substitutions) in (polyacetylene-*cis*)₅₀ oligomer on photoexcitation dynamics. (Left) Contour plots of the transition densities between the ground state ($|0\rangle$) and the first excited $1B_u$ state ($|1\rangle$) at $t = 0, 55, 83$, and ∞ fs. (Right) Variation of bond-length alternation [r_n (Å)] and compression [s_n (Å)] parameters along the polymer backbone at $t = 0, 55, 83$, and ∞ fs. On the color plots the axes are labeled by the carbon atoms along the chain, and the color map is as described in the Fig. 3 legend.

photoexcitation to higher π^* electronic orbital is possible with different dynamics. Examination of r_n and s_n confirms this conclusion. We also calculated *sp*³ chains with stronger defects that break the conjugation (such as *sp*³ defects). The results (not shown) indicate that these defects greatly enhance the localization, effectively breaking the chain into well separated pieces and limiting the dynamics to the longest conjugated region.

In our final numerical experiment, we modeled the effects of chemical substitutions by chlorinating one third of the chain, i.e., calculating a H(CH)₃₃ - (CCl)₁₇Cl oligomer. The resulting variations of r_n , s_n , and transition densities are shown in Fig. 7 Lower. Even though the bond-length alternation is increased along the chlorinated segment (Fig. 7, r_n at $t = 0$), the electronegativity of Cl effectively attracts an exciton. At $t = 0$ an excitation is already essentially localized on the substituted end. Subsequent photoexcitation dynamics occurs on the chlorinated segment. We observe strong electron coupling to C=C stretching modes at $\approx 1,620 \text{ cm}^{-1}$ (≈ 21 fs) on the chlorinated segment; whereas C=C stretching modes at $\approx 1,820 \text{ cm}^{-1}$ spatially localized along the unsubstituted part of the chain do not couple to an exciton. Subsequently, the breather period in this system is ≈ 40 fs.

Conclusion

To conclude, we modeled here photoexcitation dynamics of conjugated *cis*-polyacetylene oligomers using an ESMD quantum-chemical approach. The results show several characteristic features

of this dynamics. (i) An excitation moves to the largest conjugated segment of the polymer chain (where it has the lowest electronic energy) by means of short-range coherent localization (42) or long-range Förster transfer mechanism (58). (ii) An exciton creates phonon excitations and significant local distortions of the lattice. The C=C stretching modes exhibit the strongest coupling to the electronic system among all nuclear motions. These phonons form a complex nonlinear localized vibrational excitation (breather) that cannot be associated with any specific single linear vibrational normal mode. The subsequent dynamics is spatially localized and appears as an exchange of the energy between an exciton and a breather. (iii) The breather excitation has distinct spectroscopic signatures in the power spectra of all spectroscopic observables (such as transition frequencies and transition dipole moments, oscillator strengths), namely, a characteristic component with a period of ≈ 34 fs, which is roughly a double period of the C=C stretching motion. We observe that the breather component has the strongest signature in observables related to the intensities (transition dipoles and oscillator strengths), whereas energy variables (such as transition energies) are dominated by vibrational mode frequency components (in particular the C=C stretching mode with a period of 18.3 fs).

The magnitudes of the transient absorption spectra are related to the respective transition dipole moments and therefore contain the breather vibrational component in their power spectra, which should allow identification of breather excitations experimentally (52). Our calculated breather period of 34 fs agrees well with previous estimates for polyacetylene of 38 fs (47, 48) and 30 fs (33) obtained with the SSH models and with a recent experimental value of 44 fs (52). The breather observed in the experiment has a short lifetime of ≈ 50 fs. We can understand this dissipation by recalling that the first stage in the breather dynamics is the formation of a self-trapped exciton, which creates phonon excitations. In our simulations, phonon waves reflect from the molecular ends without

vibrational energy loss. In real samples the phonons will be scattered on the defects that limit the conjugated segment, and only a fraction of their energy will return back to the breather. Interchain interaction could enhance these dissipative processes even further. Stronger defects will be less transparent for phonons. Therefore we expect that breathers will have longer lifetimes in the defected samples. To confirm this scenario we conducted simulations on an oligomer with two defects $\text{H}(\text{CH})_{15} - \text{defect} - (\text{CH})_{30} - \text{defect} - (\text{CH})_{15}\text{H}$. A weak triple-bond (alkynyl) defect was used in one calculation, whereas a strong sp^3 (CH_2 group) defect was used in a second calculation. To simulate dissipation we damped the motion between the chain end and the defect by setting the kinetic energy of nuclei to zero at every time step. We observe that in the case of weak defects the energy dissipates on the time scale of ≈ 70 fs (i.e., the breather amplitude drops to 10% of its initial maximum value), whereas in the chain with stronger defects the breather persists up to ≈ 200 fs.

In conclusion, strong nonlinear coupling among electronic and vibrational degrees of freedom leads to a complex spatially localized photoexcited vibronic dynamics, which is a distinctive property of conjugated polymers. We expect that this dynamical excitation self-trapping process is typical for conjugated materials featuring strong electron-phonon coupling, including disordered nanomolecules. Development of ultrafast subfemtosecond spectroscopic techniques (52) and efficient quantum-chemical approaches (42, 59, 60) allows monitoring of time-dependent vibronic processes, which opens the way to understand more deeply a number of photochemical, time-dependent spectroscopic, and carrier-transport processes in electronically active soft and biological nanoscale matter.

The research at Los Alamos National Laboratory is supported by the Laboratory Directed Research and Development program of the U.S. Department of Energy. The numerical computations were performed by using the resources of the Center for Nonlinear Studies. This support is gratefully acknowledged.

- Heeger, A. J. (2001) *Rev. Mod. Phys.* **73**, 681–700.
- Friend, R. H., Gymer, R. W., Holmes, A. B., Burroughes, J. H., Marks, R. N., Taliani, C., Bradley, D. D. C., dos Santos, D. A., Brédas, J. L., Logdlund, M. & Salaneck, W. R. (1999) *Nature* **397**, 121–128.
- Braun, D. & Heeger, A. J. (1991) *Appl. Phys. Lett.* **58**, 1982–1984.
- Burn, P. L., Holmes, A. B., Kraft, A., Bradley, D. D. C., Brown, A. R., Friend, R. H. & Gymer, R. W. (1992) *Nature* **356**, 47–49.
- Burroughes, J. H., Bradley, D. D. C., Brown, A. R., Marks, R. N., Mackay, K., Friend, R. H., Burns, P. L. & Holmes, A. B. (1990) *Nature* **347**, 539–541.
- Cao, Y., Parker, I. D., Yu, G., Zhang, C. & Heeger, A. J. (1999) *Nature* **397**, 414–417.
- Gustafsson, G., Cao, Y., Treacy, G. M., Klavetter, F., Colaneri, N. & Heeger, A. J. (1992) *Nature* **357**, 477–479.
- Shen, Z. L., Burrows, P. E., Bulovic, V., Forrest, S. R. & Thompson, M. E. (1997) *Science* **276**, 2009–2011.
- Pei, Q. B., Yu, G., Zhang, C., Yang, Y. & Heeger, A. J. (1995) *Science* **269**, 1086–1088.
- Sirringhaus, H., Tessler, N. & Friend, R. H. (1998) *Science* **280**, 1741–1744.
- Ho, P. K. H., Thomas, D. S., Friend, R. H. & Tessler, N. (1999) *Science* **285**, 233–236.
- Dodabalapur, A., Bao, Z., Makhija, A., Laquindanum, J. G., Raju, V. R., Feng, Y., Katz, H. E. & Rogers, J. (1998) *Appl. Phys. Lett.* **73**, 142–144.
- Yu, G., Gao, J., Hummelen, J. C., Wudl, F. & Heeger, A. J. (1995) *Science* **270**, 1789–1791.
- Granstrom, M., Petritsch, K., Arias, A. C., Lux, A., Andersson, M. R. & Friend, R. H. (1998) *Nature* **395**, 257–260.
- Mende, L., Fechtenkötter, A., Mullen, K., Moons, E., Friend, R. H. & MacKenzie, J. D. (2001) *Science* **293**, 1119–1122.
- Yu, G., Pakbaz, K. & Heeger, A. J. (1994) *Appl. Phys. Lett.* **64**, 3422–3424.
- Yu, G., Zhang, C. & Heeger, A. J. (1994) *Appl. Phys. Lett.* **64**, 1540–1542.
- Halls, J. J. M., Walsh, C. A., Greenham, N. C., Marseglia, E. A., Friend, R. H., Moratti, S. C. & Holmes, A. B. (1995) *Nature* **376**, 498–500.
- Katz, H. E., Bao, Z. N. & Gilat, S. L. (2001) *Acc. Chem. Res.* **34**, 359–369.
- Crone, B., Dodabalapur, A., Gelperin, A., Torsi, L., Katz, H. E., Lovinger, A. J. & Bao, Z. (2001) *Appl. Phys. Lett.* **78**, 2229–2231.
- Sheraw, C. D., Zhou, L., Huang, J. R., Gundlach, D. J., Jackson, T. N., Kane, M. G., Hill, I. G., Hammond, M. S., Campi, J., Greening, B. K., Francl, J. & West, J. (2002) *Appl. Phys. Lett.* **80**, 1088–1090.
- Yang, Y. & Heeger, A. J. (1994) *Nature* **372**, 344–346.
- Wang, D. L., Gong, X., Heeger, P. S., Rininsland, F., Bazan, G. C. & Heeger, A. J. (2002) *Proc. Natl. Acad. Sci. USA* **99**, 49–53.
- Heeger, A. J., Heeger, D. J., Langan, J. & Yang, Y. (1995) *Science* **270**, 1642–1644.
- Sirringhaus, H., Kawase, T., Friend, R. H., Shimoda, T., Inbasekaran, M., Wu, W. & Woo, E. P. (2000) *Science* **290**, 2123–2126.
- Hide, F., Diaz-Garcia, M. A., Schwartz, B. J., Andersson, M. R., Pei, Q. B. & Heeger, A. J. (1996) *Science* **273**, 1833–1836.
- Tessler, N., Denton, G. J. & Friend, R. H. (1996) *Nature* **382**, 695–697.
- Frolov, S. V., Gellermann, W., Ozaki, M., Yoshino, K. & Vardeny, Z. V. (1997) *Phys. Rev. Lett.* **78**, 729–732.
- Baldo, M. A., Thompson, M. E. & Forrest, S. R. (2000) *Nature* **403**, 750–753.
- Heeger, A. J., Kivelson, S., Schrieffer, J. R. & Su, W. P. (1988) *Rev. Mod. Phys.* **60**, 781–850.
- Soos, Z. G., Ramasesha, S. & Galvao, D. S. (1993) *Phys. Rev. Lett.* **71**, 1609–1612.
- Su, W. P. & Schrieffer, J. R. (1980) *Proc. Natl. Acad. Sci. USA* **77**, 5626–5629.
- Takimoto, J. & Sasaki, M. (1989) *Phys. Rev. B* **39**, 8511–8524.
- Kirova, N., Brazovskii, S. & Bishop, A. R. (1999) *Synth. Met.* **100**, 29–53.
- Kivelson, S. & Heim, D. (1982) *Phys. Rev. B* **26**, 4278–4292.
- Frisch, M. J., Trucks, G. W., Schlegel, H. B., Scuseria, G. E., Robb, M. A., Cheeseman, J. R., Zakrzewski, V. G., Montgomery, J. A., Jr., Stratmann, R. E., Burant, J. C., et al. (2002) Gaussian 98 (Gaussian, Inc., Pittsburgh), Revision A.11.
- Szabo, A. & Ostlund, N. S. (1989) *Modern Quantum Chemistry: Introduction to Advanced Electronic Structure Theory* (McGraw-Hill, New York).
- Brédas, J. L., Cornil, J., Beljonne, D., dos Santos, D. A. & Shuai, Z. G. (1999) *Acc. Chem. Res.* **32**, 267–276.
- Tretiak, S. & Mukamel, S. (2002) *Chem. Rev.* **102**, 3171–3212.
- Cory, M. G., Zerner, M. C., Xu, X. C. & Shulten, K. (1998) *J. Phys. Chem. B* **102**, 7640–7650.
- Stratmann, R. E., Scuseria, G. E. & Frisch, M. J. (1998) *J. Chem. Phys.* **109**, 8218–8224.
- Tretiak, S., Saxena, A., Martin, R. & Bishop, A. R. (2002) *Phys. Rev. Lett.* **89**, 7402–7405.
- Tretiak, S., Saxena, A., Martin, R. & Bishop, A. R. (2002) *Phase Transitions* **75**, 725–732.
- Tsipser, E. V., Chernyak, V., Tretiak, S. & Mukamel, S. (1999) *Chem. Phys. Lett.* **302**, 77–84.
- Ridley, J. & Zerner, M. C. (1973) *Theor. Chim. Acta* **32**, 111–134.
- Dewar, M. J. S., Zöbisch, E. G., Healy, E. F. & Stewart, J. J. P. (1985) *J. Am. Chem. Soc.* **107**, 3902–3909.
- Bishop, A. R., Campbell, D. K., Lomdahl, P., Horovitz, B. & Phillipot, S. R. (1984) *Phys. Rev. Lett.* **52**, 671–674.
- Phillipot, S. R., Bishop, A. R. & Horovitz, B. (1989) *Phys. Rev. B* **40**, 1839–1855.
- Bishop, A. R., Campbell, D. K., Lomdahl, P., Horovitz, B. & Phillipot, S. R. (1984) *Synth. Met.* **9**, 223–239.
- Kress, J., Saxena, A., Bishop, A. R. & Martin, R. L. (1998) *Phys. Rev. B* **58**, 6161–6165.
- Kanner, G., Vardeny, Z., Lanzani, G. & Zheng, L. (2001) *Synth. Met.* **116**, 71–73.
- Adachi, S., Kobayashi, V. & Kobayashi, T. (2002) *Phys. Rev. Lett.* **89**, 7401–7404.
- Tretiak, S., Saxena, A., Martin, R. L. & Bishop, A. R. (2000) *Chem. Phys. Lett.* **331**, 561–568.
- Tretiak, S., Saxena, A., Martin, R. L. & Bishop, A. R. (2001) *J. Chem. Phys.* **115**, 699–707.
- Allen, M. P. & Tildesley, D. J. (1987) *Computer Simulation of Liquids* (Clarendon, Oxford).
- Mukamel, S., Tretiak, S., Wagersreiter, T. & Chernyak, V. (1997) *Science* **277**, 781–787.
- Karabunarliev, S., Baumgarten, M., Bittner, E. & Mullen, K. (2000) *J. Chem. Phys.* **113**, 11372–11381.
- Förster, T. (1946) *Naturwissenschaften* **33**, 166.
- Gai, F., Hasson, K., McDonald, J. & Anfirud, P. (1998) *Science* **279**, 1886–1891.
- Ben-Nun, M., Molnar, F., Schulten, K. & Martinez, T. (2002) *Proc. Natl. Acad. Sci. USA* **99**, 1769–1773.